



# Electrospray formation and combustion characteristics of iodine-containing Al/CuO nanothermite microparticles



Haiyang Wang<sup>a</sup>, Jeffery B. DeLisio<sup>b,c</sup>, Guoqiang Jian<sup>b,c</sup>, Wenbo Zhou<sup>b,c</sup>, Michael R. Zachariah<sup>b,c,\*</sup>

<sup>a</sup> Permanent address: Department of Safety Engineering, Nanjing University of Science and Technology, Nanjing, Jiangsu 210094, China

<sup>b</sup> Department of Chemical and Biomolecular Engineering, University of Maryland, College Park, MD 20742, United States

<sup>c</sup> Department of Chemistry and Biochemistry, University of Maryland, College Park, MD 20742, United States

## ARTICLE INFO

### Article history:

Received 23 March 2015

Received in revised form 23 March 2015

Accepted 8 April 2015

Available online 13 May 2015

### Keywords:

Nanoenergetics

Heterogeneous combustion

Metals

Thermite

## ABSTRACT

The neutralization of biologics used as components in weapon systems poses a considerable challenge. One strategy is to deliver both heat and biocidal agents simultaneously. In this paper we employ an electrospray assembly approach to create Al/CuO nanothermite microparticles containing molecular iodine ranging from 5 wt.% to 50 wt.%, and evaluate their combustion properties and potential use as sporicidal agents. The reactivity was evaluated using a constant-volume combustion cell, which showed that, with increasing iodine content, the Al/CuO/I<sub>2</sub> reaction rate is decreased by several orders of magnitude, while the burning time increased. Results also show that the reactivity of the composites can be increased by reducing the particle loading in the precursor. The post-combustion products are determined to be Al<sub>2</sub>O<sub>3</sub>, Cu and CuI. T-Jump (temperature jump) wire ignition experiments showed that the temperature for microparticles containing up to 20 wt.% of iodine are ~750 °C, which is similar to the ignition temperature of Al/CuO composites. *In-situ* rapid heating SEM imaging of Al/CuO/I<sub>2</sub> composites confirmed that iodine was released (<500 °C) prior to the thermal reaction (~800 °C). T-Jump time of flight mass spectrometry showed an early release of iodine starting at ~300 °C, and a later release ~670 °C corresponding to iodine that had been stabilized in the alumina shell of the aluminum nanoparticles during preparation of the electrospray precursor solution. The results conclude that iodine loadings of up to 50 wt.% can be stabilized within the microparticle to allow for a higher temperature iodine release along with the high temperature thermite reaction making this material a strong candidate to be used in biocidal applications.

© 2015 Published by Elsevier Inc. on behalf of The Combustion Institute.

## 1. Introduction

In a thermite reaction, a fuel (e.g., Al) and an oxidizer (CuO, Fe<sub>2</sub>O<sub>3</sub>, Bi<sub>2</sub>O<sub>3</sub>, etc.) react rapidly, producing a large quantity of thermal energy (heat) in a relatively short time (~milliseconds). What makes these materials particularly interesting is their high volumetric energy density that can be a factor of 2–3 higher than the highest energy containing organics. (e.g., TNT) [1–15]. However, the kinetics of traditional thermite formulations using micron scale particles are slow, which has recently prompted considerable interest in the use of nanoparticle precursors that can increase reactivity by as much as three orders of magnitude [16–21].

Biological-based weapons pose a significant potential threat to global security. Spores of virulent bacteria are highly stress

resistant and cannot be easily neutralized by traditional bactericide chemicals such as iodophor. Traditional thermal treatments require a relatively long time to deactivate spores [22–24]. However, it has been previously demonstrated that conventional biocidal agents such as iodine can efficiently kill spores when combined with additional heating [25]. Thus, incorporating biocidal agents into energetic material formulations that can undergo a violent thermal reaction combined with long-lasting release of sporicidal material is a viable strategy. Recently, various iodine-containing oxidizers have been developed and employed as the oxidizer component in thermite formulations that can release highly reactive-biocidal agents upon ignition [26–31]. Another, more direct approach, is to directly add biocidal agents such as iodine or silver into energetic material formulations.

The main attributes to consider when evaluating biocidal agents of this type are loading capacity of biocidal agent, speciation of the final products, and reactivity and duration of the reaction. Higher biocidal agent concentration means higher sporicidal effects. Aly

\* Corresponding author.

E-mail address: [mrz@umd.edu](mailto:mrz@umd.edu) (M.R. Zachariah).

et al. prepared Al-I<sub>2</sub> and Al-B-I<sub>2</sub> composites with iodine contents of 20 wt.% and 15 wt.%, which demonstrated an effective inactivation of aerosolized spores [32]. Secondly, the final burning products should have biocidal properties. The Al/AgIO<sub>3</sub> nanothermite has been considered as a potential biocidal agent because its main reaction products include Ag and I<sub>2</sub> [27]. I<sub>2</sub>O<sub>5</sub> has an iodine content of 76 wt.%, which can be combined with aluminum to form a highly reactive thermite that will also produce iodine [29]. In contrast, highly reactive KIO<sub>4</sub> and NaIO<sub>4</sub> also have high iodine contents and are powerful oxidants in thermite mixtures, but do not release elemental iodine as a reaction product [5]. The ideal situation entails a system that generates large amounts of heat with a long lasting and potent biocidal agent also being released.

In this work, we build on our prior efforts in microparticle assembly [33] to incorporate I<sub>2</sub> into Al/CuO nanothermite formulations using an electrospray approach to create a microparticle with 5–50 wt.% I<sub>2</sub>. Rapid-heating wire experiments and constant-volume combustion cell tests were conducted to characterize the ignition and reactivity of the composites. The compositions and morphologies of post-combustion products were collected and characterized by SEM, EDS and XRD showing major post-combustion products of Al<sub>2</sub>O<sub>3</sub>, Cu and CuI. The reaction mechanism was investigated in an *in-situ* rapid heating SEM stage and rapid heating wire ignition within the ionization and extraction region of a time of flight mass spectrometer (TOFMS).

## 2. Experimental section

### 2.1. Precursor preparation

The Al NPs were purchased from the Argonide Corporation (ALEX, ~50 nm). TGA results show they are 70 wt.% active Al, which was taken into consideration when determining the stoichiometric ratio of thermite. Both CuO NPs (<50 nm) and I<sub>2</sub> were purchased from Sigma Aldrich. The nitrocellulose (NC) used in this work was also purchased from Sigma Aldrich (4–8 wt.% Collodion solution). In a typical experiment, the CuO and Al NPs were first dispersed in acetone, and then NC and I<sub>2</sub> were added before ultrasonication of the suspension for 1.0 h. The weight percentages of iodine were varied from 5% to 50%. All the suspensions were stirred for 24 h to fully mix the Al and CuO nanoparticles. The formulations of all the samples are listed in Table 1. The particle loading is the concentration of flammable solid particles (iodine is not included) being added into the acetone during the precursor preparation process.

### 2.2. Electrospray formation

In this study the reactants were assembled into a microparticles using a previously described electrospray process [33,34]. Precursor solutions were loaded in a 10 ml syringe with a stainless steel needle (inner diameter: 0.43 mm). The syringe was controlled by a syringe pump with a constant flow rate of 4.5 ml/h. The distance between the needle and substrate is fixed at 10 cm, over which 19 kV was applied to create the electrospray and deposit the particles.

### 2.3. SEM, EDS and XRD characterization

The nanothermite samples were prepared by depositing a small amount of the powder onto a piece of carbon-tape. A Hitachi SU-70 scanning electron microscope (SEM) coupled to an EDX-spectroscopy system enables morphological and elemental characterization. X-ray Diffractometry (XRD), was obtained with a Bruker D8, using Cu K $\alpha$  radiation.

### 2.4. T-Jump ignition tests in air and in a time-of-flight mass spectrometer

The previously reported temperature jump (T-Jump) ignition method was used to ignite the samples at high heating rates that more accurately represent a combustion event. The details of these rapidly-heated wire ignition tests can be found in Refs. [5,35–37]. Typically, a thin layer of sample is coated on a small portion (3–4 mm in length) of a ~10 mm-long Pt wire (76  $\mu$ m). A current pulse of ~3 ms is applied to resistively heat the wire to ~1800 K at a heating rate of ~5  $\times 10^5$  K s<sup>-1</sup>. The temporal wire temperature is determined from the resistance by simultaneously monitoring the current and voltage. Images of the thermite burning on the wire in air were recorded using a Vision Research Phantom v12.0 high-speed digital camera, with the resolution set at 256  $\times$  256 pixels and a frame rate of 67,065 fps (14.9  $\mu$ s per frame).

This same rapidly-heated wire ignition method was used within a time of flight mass spectrometer (TOFMS) to perform temporally resolved temperature and speciation analysis. The extraction region of the TOFMS was pulsed at 10 kHz resulting in a mass spectrum every 0.1 ms.

### 2.5. Combustion cell tests

The details of combustion cell experiment can be found in Refs. [5,36]. In this study, 25.0 mg of loose thermite powder was placed inside a cell with a constant-volume (~13 cm<sup>3</sup>), and was ignited using a resistively heated nichrome coil. A piezoelectric pressure sensor (PCB) along with an in-line charge amplifier and signal conditioner were used to record the pressure history. A planoconvex lens ( $f = 50$  mm) and a photodetector were used to collect the time resolved optical emission from the reaction. The burning time was defined as peak width at half height of the optical emission.

### 2.6. Rapid heating stage on SEM

A specially designed sample holder (Aduro holder, Protochips, Inc.) was used to heat samples *in situ* within a scanning electron microscopy (SEM, Hitachi, SU-70 FEG-SEM) at a rate of ~1  $\times 10^6$  K s<sup>-1</sup> [38]. For these studies the sample was heated on the hot-stage, from room temperature to 500 °C and held at temperature for 10 ms, then allowed to cool to room temperature (RT). It was then heated again to 800 °C for 10 ms, cooled again, and finally heated to 1000 °C for 10 ms. SEM images were taken before and after each heating step.

**Table 1**  
Thermite formulations.

Thermite	Particle loading (mg/ml)	Al (mg)	CuO (mg)	Acetone (mL)	Nitrocellulose (mg)	Iodine (mg)
Al/CuO/NC thermite	83	47.5	142.5	2.4	10	0
	250	47.5	142.5	0.8	10	0
Al/CuO/NC/I <sub>2</sub> thermite	83	47.5	142.5	2.4	10	10–200
	250	47.5	142.5	0.8	10	10–200

mg/ml = mass of solid in ml of acetone.

### 3. Results and discussion

#### 3.1. Electro spray formation of Al/CuO/I<sub>2</sub> composites

From our previous studies we have found electro spray to be a facile granulating technology, which can assemble nanoparticles into micro-sized particles with a porous interior structure. In this technique, an electrohydrodynamic jet breakup results in the formation of a fine spray containing dispersed NP's, and other dissolved materials, which upon solvent evaporation form micro-sized particles. In our previous studies [33,34] we have used this electro spray approach to create a micro-sized Al and Al/CuO composites (5 wt.% NC) that have demonstrated enhanced reactivity. In the present study, we incorporate elemental iodine into the thermite formulation to create reactive iodine-containing composites.

SEM images of electro sprayed Al/CuO composites with iodine displayed microparticles with a wide size distribution spanning ~5 μm to ~20 μm. Iodine crystals are also observed in the particle, as seen in Fig. 1a–d, and are formed upon solvent evaporation from the electro sprayed droplets. The particles have a more porous and open structure than we have previous observed in the Al/CuO [33] composites implying that the iodine interferes with the compaction aspect of assembly of the nanoparticles. This is possibly due to the larger sized (micron) sheet-like iodine crystals

disrupting the gelling process of the nanoparticles during solvent evaporation [39].

Figure 1a and b shows the Al/CuO composites with different iodine content produced by electro spray with a precursor particle loading of 250 mg/ml. From a comparison of Fig. 1a and b, it is clear that distinct crystals of I<sub>2</sub> are formed that increase in size from sub-micron to micron as the iodine content increase from 20 wt.% to 40 wt.%. Lowering the particle loading to 83 mg/ml as shown in Fig. 1c and d, appears to improve the dispersion of the Al and CuO nanoparticles, as well as the iodine crystals as evidenced by EDS imaging. Moreover, compared to the sample with the 250 mg/ml particle loading case, the iodine crystals are much smaller (<200 nm, Fig. 1d).

#### 3.2. Reactivity of Al/CuO/I<sub>2</sub> composites

The reactivity of iodine containing Al/CuO composites was characterized in a constant volume combustion cell [5,36]. The peak pressure and burning time of composites with different particle loading and different iodine content are shown in Fig. 2.

Peak pressure is very sensitive to iodine content, and drops dramatically with only a 5% addition of iodine. The peak pressure of ~1200 kPa for the low particle loading case, is 5× higher than the high particle loading, with 5 wt.% iodine. Further increases in iodine loading in the precursor solution appears to have

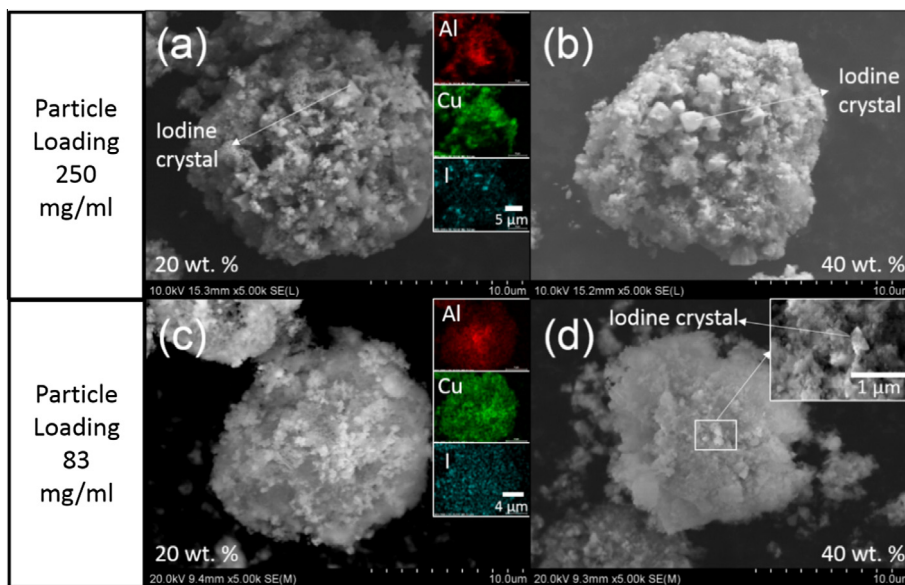


Fig. 1. SEM images of iodine-containing Al/CuO composites. Iodine content: 20 wt.%, (a, c), 40 wt.% (b, d). Note: a and b are microparticles from precursors with particle loading of 250 mg/ml; (c) and (d) are from precursors with particle loading of 83 mg/ml. The inserts in (a) and (c) are EDS elemental maps.

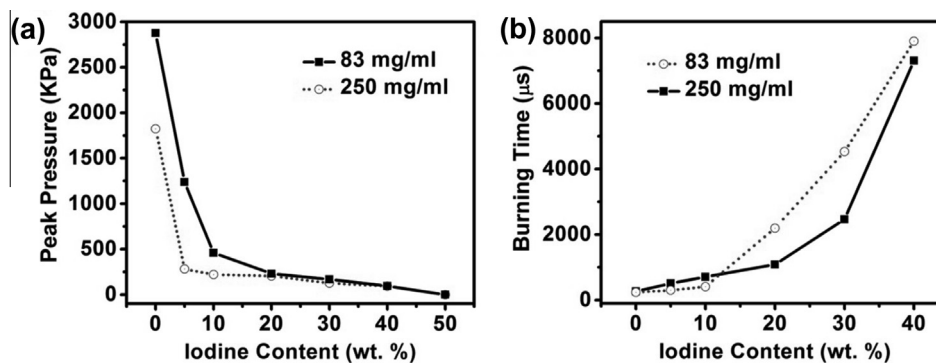
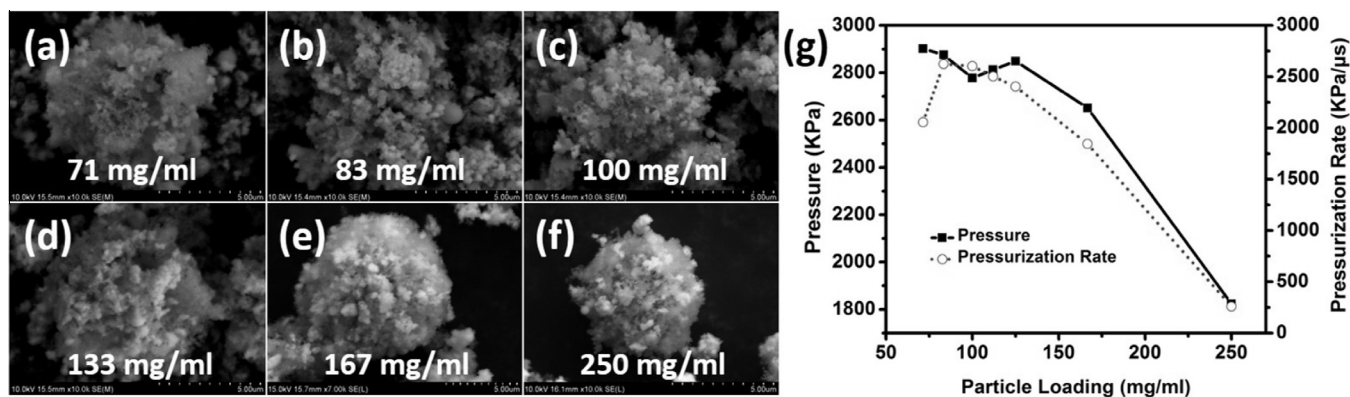


Fig. 2. Peak pressure and burn time as a function of iodine content. Note: 50 wt.% iodine case can be ignited but is too weak to obtain an optical signal.



**Fig. 3.** The SEM images of Al/CuO composites with different precursor solution particle loading (a–f); the peak pressure and pressurization rate changing with particle loading in precursors (g). Note: NC is 5 wt.% in all composites.

**Table 2**

Pressure and pressurization rate of Al/CuO composites with different particle loadings. Note: all composites contain 5 wt.% NC.

Particle loading (mg/ml)	Al/CuO composites		Al/CuO composites with 10 wt.% iodine	
	Pressure (kPa)	Pressurization rate (kPa/μs)	Pressure (kPa)	Pressurization rate (kPa/μs)
250	1820	260	160	0.1
167	2650	1840	390	2
83	2880	2620	570	14

diminished impact on the peak pressure. The microparticles created at the higher 250 mg/ml particle loading perform more poorly, initially, but asymptote to essentially the same values with increasing iodine loading from 10 wt.% to 50 wt.%. The burning times increase dramatically with increasing iodine content, but appear to be relatively insensitive to loading when iodine content is higher than 10 wt.%.

To further evaluate the role of particle loading on the microparticle's morphology and reactivity, Al/CuO composites without iodine were prepared. SEM images are shown in Fig. 3a–f, and the peak pressure and pressurization rate are listed and plotted in Table 2 and Fig. 3g. The general trend appears to be that particle loading does have a significant impact, and lower particle concentrations in the electrospray precursor lead to higher reactivity particles. The reasons for this trend are, at this point, unclear, but the SEM images do seem to suggest a more dense structure for the particles created at high loadings.

The iodine containing Al/CuO composites were also ignited using the T-Jump resistively heated Pt wire to obtain the ignition temperature in air using high speed video, which is displayed in Fig. 4. Visibly weaker burning is observed with an increase in iodine content from 0 wt.% to 20 wt.%. Ignition temperature was found to be  $\sim 750$  °C for both the 10 wt.% and 20 wt.% iodine cases and similar to the physical mixed Al/CuO nanothermite [9]. Thus iodine has no impact on the point of ignition, but clearly impedes combustion.

### 3.3. Post combustion analysis

Post-combustion analysis can provide important clues used to evaluate the reactivity of a thermite. Highly reactive thermites yield high pressure and thermal energy to vaporize the burning products, and thus should show a small particle size residue post-combustion. In contrast, a weak thermite should form large aggregates with an uneven dispersion of elements. Post-combustion products from the two thermites (high and low loadings) were collected and characterized by SEM and EDS elemental mapping.

Recall from Fig. 3 and Table 2 that high particle loadings decrease performance, and that iodine dispersion was found to be less homogeneous. As Fig. 5 reveals, the post-combustion residues (Fig. 5a and b) of the high particle loadings case are mostly 3–5 μm while those in low particle loadings case are primarily less than 1 μm (Fig. 5c and d). EDS elemental mapping results are consistent in showing that at lower particle loadings, the distribution

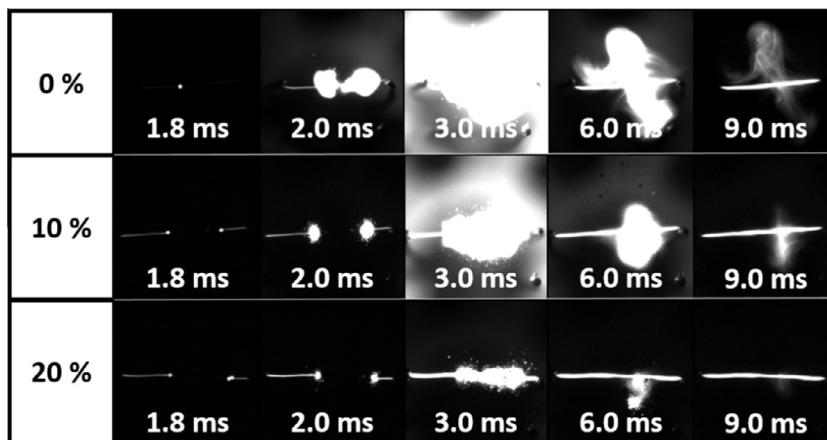


**Fig. 4.** Burning snapshots on T-Jump wire of Al/CuO composites. Iodine content: 0 wt.%, 10 wt.% and 20 wt.%. Note: particle loading, 250 mg/ml.

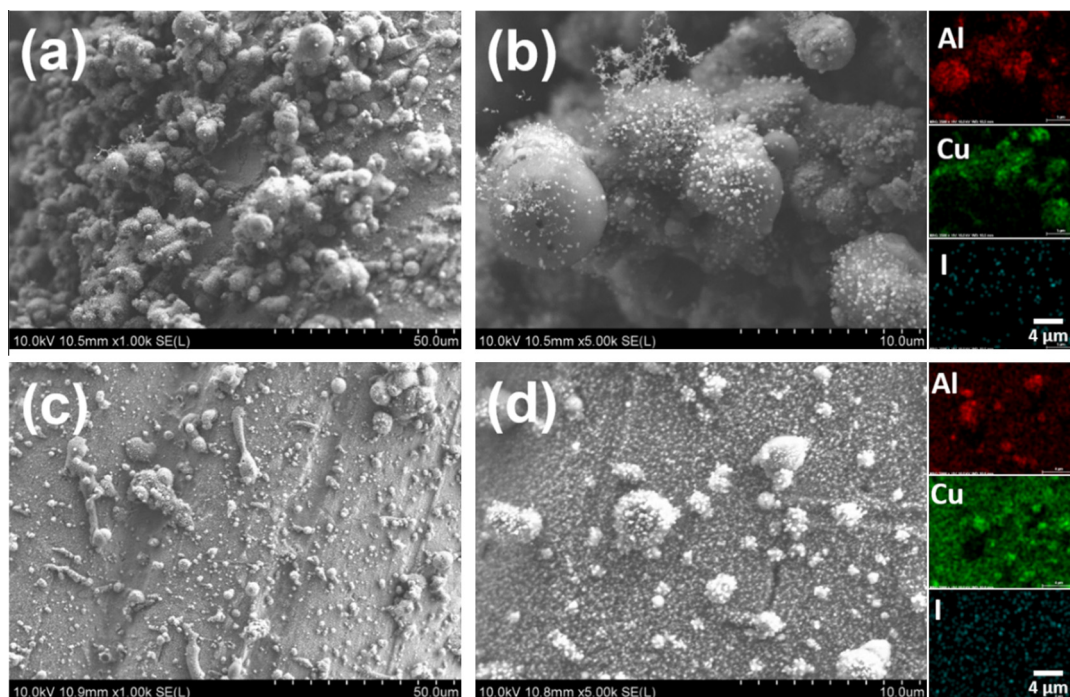


**Fig. 5.** The SEM images (a–d) and EDS elemental mapping results (for b and d) of the burned products from different particle loading Al/CuO composites. Particle loading: 250 mg/ml (a, b); 83 mg/ml (c, d).

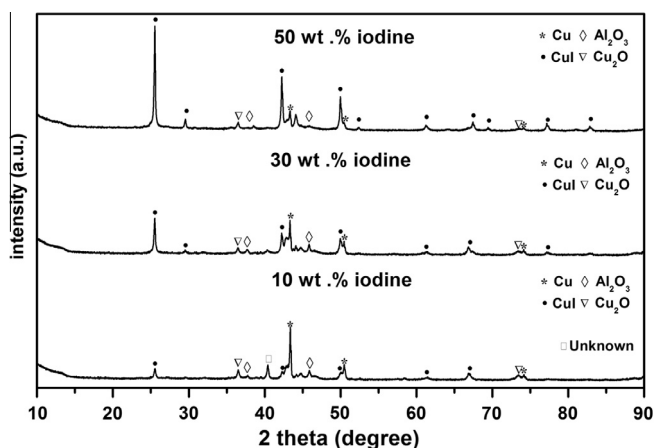


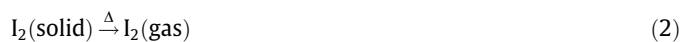
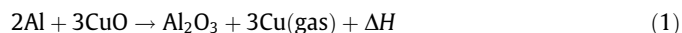
**Fig. 6.** XRD patterns of combustion products from different Al/CuO composites with iodine contents of 10 wt.%, 30 wt.% and 50 wt.%. Note: JCPDS No. for Cu is 04-0836, for  $\text{Al}_2\text{O}_3$  is 46-1131, for CuI is 83-1105 and for  $\text{Cu}_2\text{O}$  is 78-2076.

of elements is more homogeneous. We also observe a more homogenous elemental distribution of Al, Cu and I in the low particle loading case. This result is consistent with the trends seen in Table 2, where the high loading case (250 mg/ml) presented the poorest combustion performance, and results in combustion products that are large (Fig. 5a and b).

The rapid decrease in reactivity of iodine-containing Al/CuO composites with the increase of iodine content may be attributable to two main factors. Firstly, the iodine might coat the NP's or form crystals during the assembly process, i.e. the spaces left between Al and CuO NPs after iodine volatilization may impede the condensed-state reaction between Al and CuO by decreasing the interfacial contact and increasing diffusion distances. Secondly, iodine is a passive agent and thus acts as a heat sink. The sublimation of iodine from solid to gas is an endothermic process. However, an adiabatic combustion temperature calculation for Al/CuO composites with different iodine content shows only a

350 °C decrease in temperature for a 50 wt.% iodine addition. More relevant, perhaps, is that a significant degradation in performance was observed with only a 5% iodine addition (see Fig. 2), which should have only a minimal effect on the adiabatic flame temperature, thus it seems reasonable to conclude that iodine's effect on combustion is a kinetic limitation.

The burning products were also characterized by XRD to determine product composition. Diffraction spectra shown in Fig. 6 indicate the presence of Cu,  $\text{Al}_2\text{O}_3$ ,  $\text{Cu}_2\text{O}$  and CuI, which are the primary species produced in the combustion cell, indicating a two stage mechanism for the iodine containing thermite reaction that proceeds as follows: (1) thermite reaction between Al and CuO produce heat to vaporize Cu and  $\text{I}_2$ ; (2) The vaporized gas phase product Cu reacts with gaseous  $\text{I}_2$  to form CuI.



In the second stage of the reaction, Cu is always in excess for these samples on a mole basis, therefore the amount of CuI produced was limited by the amount of iodine. As shown in Fig. 6, the 50 wt.% iodine sample has strongest CuI signal while the 10 wt.% iodine sample has the strongest Cu signal. Despite the fact that iodine reacts with copper, it has been reported that CuI nanoparticles also have significant biocidal performance [40–43].

#### 3.4. Reaction mechanism under rapid heating conditions

Iodine containing Al/CuO composite (30 wt.%) were heated *in-situ* on a SEM stage at a heating rate of  $\sim 1 \times 10^6 \text{ K s}^{-1}$ . The behavior of the particle morphology with temperature was shown in Fig. 7. The rods in the composites (original) are the iodine crystals that have disappeared at 500 °C heating for 10 ms. This is consistent with the fact that the boiling point of iodine is 183 °C. The redox reaction between Al and CuO has already commenced at

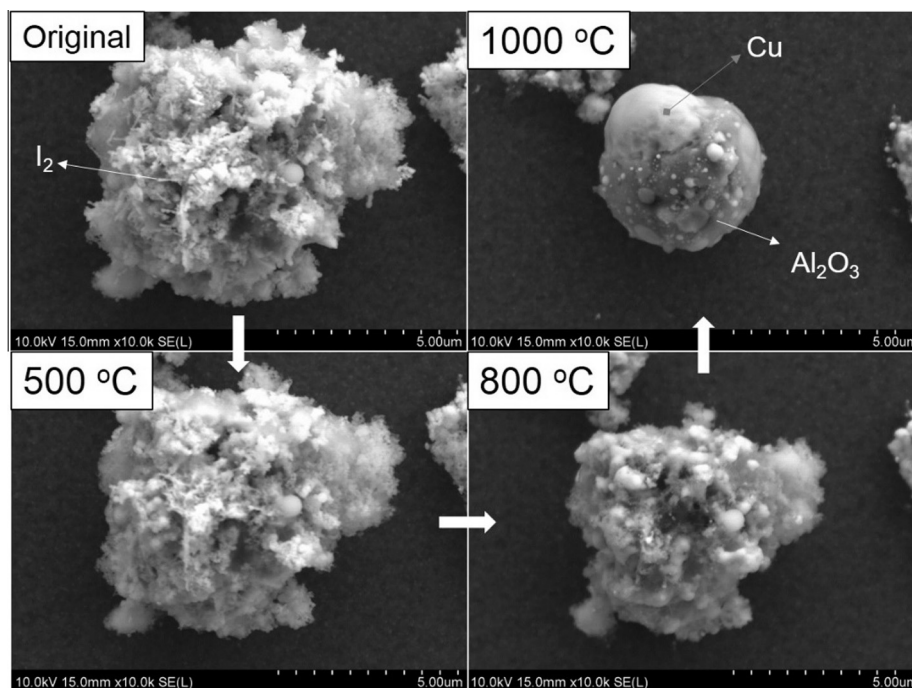


Fig. 7. The morphological changes of iodine containing Al/CuO composites (30 wt.% iodine) during rapid heating with a fast heating stage SEM (heating duration: 10 ms).

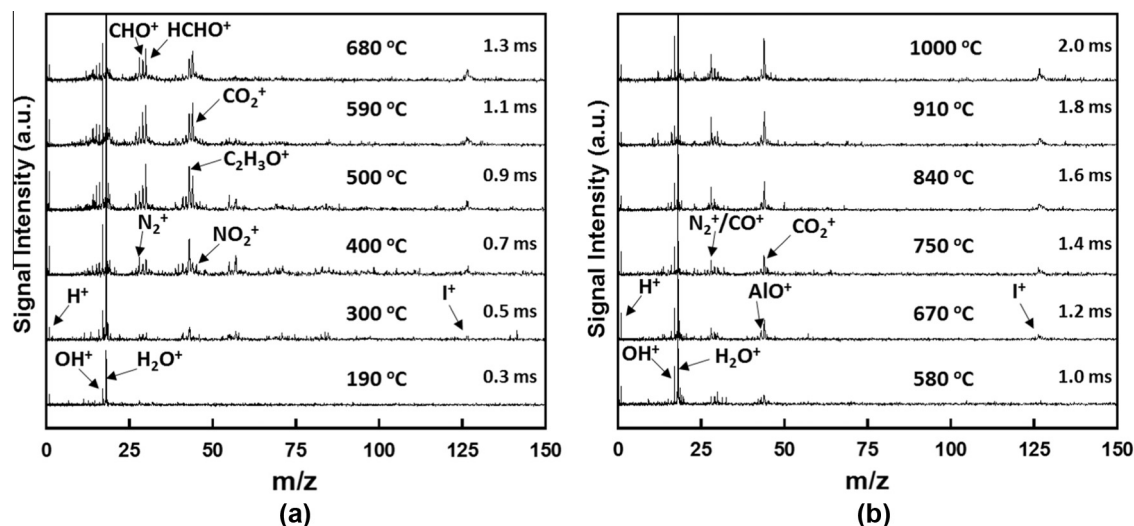


Fig. 8. T-jump mass spectrum of iodine containing Al/CuO (50 wt.% iodine) composites on rapidly heated wire ( $\sim 5 \times 10^5$  K/s) for (a) samples directly electrospayed onto the wire and (b) sampled suspended in hexane and then deposited onto the wire. Note: the labeled is the time and corresponding temperature after triggering.

800 °C, where small Cu aggregates show up in the composite. After heating the composites to 1000 °C for 10 ms, the reaction appears to be near completion, forming Cu and  $\text{Al}_2\text{O}_3$  aggregates.

The iodine containing Al/CuO composites were ignited on a rapidly heated platinum (Pt) wire in a Time of Flight Mass Spectrometer to determine the species produced (heating rate:  $\sim 5 \times 10^5$  K  $\text{s}^{-1}$ ) [5,35,37]. Two different sample deposition methods were employed to analyze the release of iodine in the 50 wt.%  $\text{I}_2$  Al/CuO microparticles. Figure 8a shows the time resolved mass spectra with corresponding wire temperatures for the case where the sample was directly electrospayed onto the Pt wire used for ignition. In Fig. 8b, the microparticles were dispersed in hexane, dissolving any elemental  $\text{I}_2$  crystals in the structure, and then deposited onto the Pt wire.

Iodine appears much earlier ( $\sim 300$  °C) in the experiment where the particles were directly electrospayed onto the wire (Fig. 8a).

This initial iodine release corresponds to the sublimation of the  $\text{I}_2$  crystals within the microparticles. This could be occurring at a slightly higher temperature than the boiling point of iodine due to the high heating rates ( $\sim 5 \times 10^5$  K/s) used and the iodine potentially being trapped in the NC matrix, which decomposes at  $\sim 170$  °C. The NC decomposition products  $\text{N}_2^+$ ,  $\text{C}_2\text{H}_3\text{O}^+$ ,  $\text{CHO}^+$ ,  $\text{HCHO}^+$  and  $\text{NO}_2^+$  are apparent in the mass spectra starting at 300 °C, the same temperature at which iodine is first detected. The late appearance of iodine in the time resolved mass spectra for the sample washed in hexane alludes to a second stage of iodine release in these samples. This iodine release occurs at 670 °C, which is close to the measured ignition temperature of the microparticles in air.  $\text{AlO}$  is also detected at this time validating that oxidation of aluminum is occurring concurrently with the release of iodine. It is proposed that during the sample preparation process, some percentage of iodine dopes the alumina ( $\text{Al}_2\text{O}_3$ ) shell

of the Al NPs. This result is consistent with previous work showing that metal oxides (e.g.  $\text{TiO}_2$ ) can be doped with iodine due to the electrostatic interactions between partially polarizable molecular iodine and the metal oxide [44]. In these iodine containing Al/CuO composites, iodine is likely stabilized by the  $\text{Al}_2\text{O}_3$  shell of the aluminum nanoparticles and is not released until the shell is disrupted by the melting of the aluminum core [45].

To evaluate this issue further, X-ray photoelectron spectroscopy (XPS) was performed on Al,  $\text{Al}_2\text{O}_3$ , and copper oxide (CuO), NPs, all of which were exposed to iodine in the same fashion as the precursor solution. The solvent was removed by heating the samples under vacuum, which would also sublime any excess iodine that had recrystallized. There was no evidence of Al–I or Cu–I bonds present, but atomic iodine was present in all three samples. We did find however, that highest iodine content was found in the Al NP. The  $\text{Al}_2\text{O}_3$  nanopowder used in the XPS study was crystalline and had a lower aluminum to iodine atomic ratio than the aluminum nanoparticles. We conjecture that iodine must be electrostatically stabilized in the oxide shell of the Al nanopowder which is amorphous.

#### 4. Conclusion

Iodine was successfully incorporated into Al/CuO nanothermite composites and their combustion properties were characterized. With the increase of the iodine content, the reactivity of the nanothermite composites was reduced, while the burn time observed an exponential increase. The post-combustion product of the iodine-containing Al/CuO composites was found to be  $\text{Al}_2\text{O}_3$ , Cu,  $\text{Cu}_2\text{O}$  and CuI. The reaction mechanism of iodine-containing Al/CuO composites was systemically investigated. Through the rapid heating experiments performed in SEM and TOFMS, the iodine was found to be released starting at 300 °C. A second release of iodine was observed starting at 670 °C, which is close to that of the Al/CuO ignition temperature, indicating that the addition of iodine does not significantly impede initiation of this reaction. The high temperature iodine release is attributed to some percentage of iodine doping the alumina shell of the Al NPs in the composite during preparation of the electrospray precursor solution. The fact that iodine is released at a high temperature leads toward the conclusion that this material could efficiently inactivate spores with an almost simultaneous release of bactericide and heat/pressure. Moreover, the employed electrospray process can allow for a large fraction of iodine to be added into Al/CuO formula. It was found that 50 wt.% iodine in Al/CuO will not reduce the ignition temperature significantly. The iodine-containing Al/CuO composites are a clear candidate to be used in a biocidal agent due to their adjustable reactivity and iodine content.

#### Acknowledgments

This work was supported by the Defense Threat Reduction Agency and the Army Research Office. We acknowledge the support of the Maryland Nanocenter and its NispLab. The NispLab is supported in part by the NSF as a MRSEC Shared Experimental Facility. Haiyang Wang is grateful for the financial support from China Scholarship Council.

#### References

- [1] C. Rossi, A. Estève, P. Vashishta, *J. Phys. Chem. Solids* 71 (2010) 57.
- [2] M.R. Weismiller, J.Y. Malchi, J.G. Lee, R.A. Yetter, T.J. Foley, *Proc. Combust. Inst.* 33 (2011) 1989.

- [3] K. Moore, M.L. Pantoya, S.F. Son, *J. Propul. Power* 23 (2007) 181.
- [4] M.L. Pantoya, J.J. Granier, *Propellants, Explos., Pyrotech.* 30 (2005) 53.
- [5] G.Q. Jian, J.Y. Feng, R.J. Jacob, G.C. Egan, M.R. Zachariah, *Angew. Chem. Int. Ed.* 52 (2013) 9743.
- [6] J.J. Granier, M.L. Pantoya, *Combust. Flame* 138 (2004) 373.
- [7] K.J. Blobaum, M.E. Reiss, J.M. Plitzko, T.P. Weihs, *J. Appl. Phys.* 94 (2003) 2915.
- [8] M. Schoenitz, T.S. Ward, E.L. Dreizin, *Proc. Combust. Inst.* 30 (2005) 2071.
- [9] K.J. Blobaum, A.J. Wagner, J.M. Plitzko, D. Van Heerden, D.H. Fairbrother, T.P. Weihs, *J. Appl. Phys.* 94 (2003) 2923.
- [10] M. Petrantonio, C. Rossi, L. Salvagnac, V. Conédéra, A. Estève, C. Tenailleau, P. Alphonse, Y.J. Chabal, *J. Appl. Phys.* 108 (2010) 084323.
- [11] K. Zhang, C. Rossi, G.A. Ardila Rodriguez, *Appl. Phys. Lett.* 91 (2007) 113117.
- [12] S.M. Umbrajkar, S. Seshadri, M. Schoenitz, V.K. Hoffmann, E.L. Dreizin, *J. Propul. Power* 24 (2008) 192.
- [13] T.S. Ward, W. Chen, M. Schoenitz, R.N. Dave, E.L. Dreizin, *Acta Mater.* 53 (2005) 2909.
- [14] S.H. Kim, M.R. Zachariah, *Adv. Mater.* 16 (2004) 1821.
- [15] T.M. Tillotson, A.E. Gash, R.L. Simpson, L.W. Hrubesh, J.H. Satcher Jr., J.F. Poco, *J. Non-Cryst. Solids* 285 (2001) 338.
- [16] H.S. Seo, J.K. Kim, J.W. Kim, H.S. Kim, K.K. Koo, *J. Ind. Eng. Chem.* 20 (2014) 189.
- [17] C. Rossi, K. Zhang, D. Esteve, P. Alphonse, P. Tailhades, C. Vahlas, *Microelectromech. Syst.* 16 (2007) 919.
- [18] S. Subramaniam, S. Hasan, S. Bhattacharya, Y. Gao, S. Apperson, M. Hossain, R.V. Shede, S. Gangopadhyay, R. Render, P. Kapper, S. Nicolich, *MRS Proc.* 896 (2005) 9.
- [19] R. Shende, S. Subramanian, S. Hasan, S. Apperson, R. Thiruvengadathan, K. Gangopadhyay, S. Gangopadhyay, P. Redner, D. Kapoor, S. Nicolich, W. Balas, *Propellants, Explos., Pyrotech.* 33 (2008) 122.
- [20] J.Y. Malchi, T.J. Foley, R.A. Yetter, *ACS Appl. Mater. Interfaces* 1 (2009) 2420.
- [21] F. Séverac, P. Alphonse, A. Estève, A. Bancaud, C. Rossi, *Adv. Funct. Mater.* 22 (2012) 323.
- [22] W.L. Nicholson, N. Munakata, G. Horneck, H.J. Melosh, P. Setlow, *Microbiol. Mol. Biol. Rev.* 64 (2000) 548.
- [23] P. Setlow, *J. Appl. Microbiol.* 101 (2006) 514.
- [24] M.J. Leggett, G. McDonnell, S.P. Denyer, P. Setlow, J.Y. Maillard, *J. Appl. Microbiol.* 113 (2012) 485.
- [25] O. Mulamba, M. Pantoya, E. Hunt, Thermal influences on the neutralization of spore forming bacteria, in: Paper presented at ASME 2012 Heat Transfer Summer Conference collocated with the ASME 2012 Fluids Engineering Summer Meeting and the ASME 2012 10th International Conference on Nanochannels, Microchannels, and Minichannels July 8–12, 2012, Rio Grande, Puerto Rico, USA.
- [26] C.E. Johnson, K.T. Higa, Presented at MRS Proc. Iodine-Rich Biocidal Reactive Materials, Boston, vol. 11, 2012, pp. 25–30.
- [27] O. Mulamba, E.M. Hunt, M.L. Pantoya, *Biotechnol. Bioprocess Eng.* 18 (2013) 918.
- [28] C. He, J. Zhang, J.M. Shreeve, *Chem. – Eur. J.* 19 (2013) 7503.
- [29] J. Feng, G. Jian, Q. Liu, M.R. Zachariah, *ACS Appl. Mater. Interfaces* 5 (2013) 8875.
- [30] K.T. Sullivan, N.W. Piekiel, S. Chowdhury, C. Wu, M.R. Zachariah, C.E. Johnson, *Combust. Sci. Technol.* 183 (2010) 285.
- [31] J.W. Tringe, S.E. Létant, L.C. Dugan, H.W. Levie, A.L. Kuhl, G.A. Murphy, M.L. Pantoya, *J. Appl. Phys.* 114 (2013) 234903.
- [32] Y. Aly, S. Zhang, M. Schoenitz, V.K. Hoffmann, E.L. Dreizin, M. Yermakov, R. Indugula, S.A. Grinshpun, *Combust. Flame* 161 (2014) 303.
- [33] H.Y. Wang, G.Q. Jian, G.C. Egan, M.R. Zachariah, *Combust. Flame* 161 (2014) 2203.
- [34] H.Y. Wang, G.Q. Jian, S. Yan, J.B. DeLisio, C. Huang, M.R. Zachariah, *ACS Appl. Mater. Interfaces* 5 (2013) 6797.
- [35] G.Q. Jian, S. Chowdhury, K. Sullivan, M.R. Zachariah, *Combust. Flame* 160 (2013) 432.
- [36] K. Sullivan, M.R. Zachariah, *J. Propul. Power* 26 (2010) 467.
- [37] G.Q. Jian, N.W. Piekiel, M.R. Zachariah, *J. Phys. Chem. C* 116 (2012) 26881.
- [38] K.T. Sullivan, W.A. Chiou, R. Fiore, M.R. Zachariah, *Appl. Phys. Lett.* 97 (2010) 133104.
- [39] C. Zangmeister, J. Radney, L.T. Dockery, J.T. Young, X. Ma, R. You, M.R. Zachariah, *Proc. Natl. Acad. Sci.* 111 (2014) 9037.
- [40] Y. Fujimori, T. Sato, T. Hayata, T. Nagao, M. Nakayama, T. Nakayama, K. Suzuki, *Appl. Environ. Microbiol.* 78 (2012) 951.
- [41] J.B. Cross, R.P. Currier, D.J. Torraco, L.A. Vanderberg, G.L. Wagner, P.D. Gladen, *Appl. Environ. Microbiol.* 69 (2003) 2245.
- [42] N. Shionoiri, T. Sato, Y. Fujimori, T. Nakayama, M. Nemoto, T. Matsunaga, T. Tanaka, *J. Biosci. Bioeng.* 113 (2012) 580.
- [43] A. Pramanik, D. Laha, D. Bhattacharya, P. Pramanik, P. Karmakar, *Colloids Surf., B* 96 (2012) 50.
- [44] G. Liu, C. Sun, L. Wang, S.C. Smith, G.Q. Lu, H. Cheng, *J. Mater. Chem.* 21 (2011) 14672.
- [45] S. Zhang, C. Badiola, M. Schoenitz, E.L. Dreizin, *Combust. Flame* 159 (2012) 1980.